Journal of Power Sources 206 (2012) 222–229

Contents lists available at SciVerse ScienceDirect

Journal of Power Sources

journal homepage: www.elsevier.com/locate/jpowsour

Preparation of carbon-coated $LiFe_{0.2}Mn_{0.8}PO_4$ cathode material and its application in a novel battery with $Li_4Ti_5O_{12}$ anode

Qing-Qing Zou, Guan-Nan Zhu, Yong-Yao Xia *

Department of Chemistry and Shanghai Key Laboratory of Molecular Catalysis and Innovative Materials, Institute of New Energy, Fudan University, Shanghai 200433, China

ARTICLE INFO

Article history:
Received 21 October 2011
Received in revised form
22 December 2011
Accepted 23 December 2011
Available online 23 January 2012

Keywords:
Lithium manganese phosphate
Lithium titanate
Carbon coating
Li-ion batteries

ABSTRACT

$LiFe_{0.2}Mn_{0.8}PO_4$ has been prepared by a solid state reaction process in combination with a ball-milling with carbon black and sucrose as carbon sources. The effects of the ratio of carbon precursors, the total carbon content, and ball-milling time on the physico-chemical and electrochemical properties of C-$LiFe_{0.2}Mn_{0.8}PO_4$ are extensively studied. Under the optimal condition, the as-prepared Li $Fe_{0.2}Mn_{0.8}PO_4$ gives a capacity of 150 mAh g^{-1} at 1/20*C* and 110 mAh g^{-1} at 1*C*. A novel lithium-ion battery consisting of $LiFe_{0.2}Mn_{0.8}PO_4$ cathode, $Li_4Ti_5O_{12}$ anode delivers a capacity of 70 mAh g^{-1} and a specific energy of 170 Wh kg^{-1} with an output voltage of 2.45 V based on the total weight of both active electrode materials. The cell also exhibits an excellent cycling stability with a capacity retention of 92% over 200 charge/discharge cycles.

1. Introduction

$LiFePO_4$ has been demonstrated to be one of the most promising cathode materials for lithium-ion batteries, especially for large-scale applications, such as plug-in hybrid vehicles and stationary powers, because of the inherent low cost, nontoxicity, and extremely high stability [1–3]. However, the specific energy of $LiFePO_4$ is still lower compared with the conventional LIB (lithium-ion battery) using $LiCoO_2$ and $LiMn_2O_4$ because of the low relative redox voltage of 3.5 V versus Li/Li^+. $LiMnPO_4$ is a much more promising cathode material for lithium-ion batteries than $LiFePO_4$ because of its higher redox voltage of 4.2 V versus Li/Li^+. However, $LiMnPO_4$ also suffers from poor Li^+ intercalation (deintercalation) kinetics due to its intrinsically low ionic and electronic conductivity. The electronic conductivity of LiMnPO4 is $<10^{-10}$ S cm^{-1} as compared with 1.8×10^{-8} S cm^{-1} for $LiFePO_4$ [4,5]. The performance of the $LiMnPO_4$ electrode has been improved by doping it with iron atoms or nanosized particles or by carbon coating [6–14]. In 2001, Yamada et al. synthesized $LiFe_{0.4}Mn_{0.6}PO_4$, showing a large capacity of 160 mAh g^{-1} [15,16]. In 2009, Aurbach et al. reported carbon-coated $LiFe_{0.2}Mn_{0.8}PO_4$ with a reversible capacity of 165 mAh g^{-1} at *C*/20 [17]. Huang et al. prepared a carbon-coated mesoporous $LiFe_{0.2}Mn_{0.8}PO_4$ solid solution with capacities of 140 mAh g^{-1} at 1/20*C* and 80 mAh g^{-1} at 2*C* [18]. The nanosized particles reduce the solid-state diffusion path, thus expediting the lithium-ion transport by overcoming the kinetic limitation. Additionally, the relatively high surface area for the nanosized particles promotes fast charge transfer [19,20] and a uniform carbon coating on the particle surface enhances the electronic conductivity, allowing fast electrons to tunnel among the active materials. Preparation of carbon coated nanosized particles is undoubtedly the most promising approach to improve the poor rate capability of the electrode materials resulting from low electronic conductivity and poor ionic transport. It is well known that $LiMnPO_4$ is thermodynamically less stable than $LiFePO_4$ and that the preparation temperature of $LiMnPO_4$ is much lower than that of $LiFePO_4$ [7]. Similar to $LiFePO_4$, sucrose has typically been used to protect Mn^{2+} from oxidation and particle aggregation, but $LiMnPO_4$ shows poor electronic conductivity due to the low temperature of the reaction [21,22]. Carbon with good electronic conductivity is usually added to $LiMnPO_4$. However, very few studies have been focused on this direction.

In the present work, we report the synthesis and electrochemical performance of a nanostructured carbon-$LiFe_{0.2}Mn_{0.8}PO_4$ nanocomposite prepared by solid-state reaction followed by ball milling. The effect of the carbon (C) amount and the particle size on the physiochemical and electrochemical properties of C-$LiFe_{0.2}Mn_{0.8}PO_4$ was extensively studied. We also investigated the battery performance of a new battery system based on the $LiFe_{0.2}Mn_{0.8}PO_4$ as a positive electrode and lithium titanate $Li_4Ti_5O_{12}$ as a negative electrode.

2. Experimental

The C-$LiFe_{0.2}Mn_{0.8}PO_4$ compound was synthesized by a solid-state reaction. Stoichiometric amounts of $MnCO_3$ (Aldrich, 99.9%),

* Corresponding author. Tel.: +86 21 51630318; fax: +86 21 51630318.
E-mail address: yyxia@fudan.edu.cn (Y.-Y. Xia).

0378-7753/$ – see front matter © 2012 Elsevier B.V. All rights reserved.
doi:10.1016/j.jpowsour.2011.12.050

$Fe(C_2O_4)\cdot 2H_2O$ (Aldrich, 99%) and LiH_2PO_4 (Sinopharm Chemical Reagent Co., Ltd.) were mixed thoroughly with carbon black and sucrose (Sinopharm Chemical Reagent Co., Ltd.). The mixture was reground by high-energy ball milling for several hours under Ar protection, followed by calcination at 550 °C for 3 h in an argon–hydrogen atmosphere (95/5, v/v). The carbon-coated $Li_4Ti_5O_{12}$ was prepared by the following process, as reported previously [21]. Anatase TiO_2 (AR, Zhoushan Mingri New Material Co. Ltd.) and sugar as a carbon source (AR, Shanghai Chemical Agents Co. Ltd.) were mixed in alcohol with a weight ratio of 10:3 and stirred for 1 h, followed by overnight drying at 100 °C. The mixture was heat treated at 600 °C for 5 h under N_2 flow of 0.7 L min^{-1} for the carbonization of sugar. Then the resulted carbon-coated TiO_2 was ball milled with Li_2CO_3 as a lithium salt (99.5%, Shanghai Chemical Agents Co. Ltd.) with a Li:Ti molar ratio 4:5 in a ball milling machine (Fritsch Pulverisette 6) to form a slurry, which was then spray-dried for sphere-making. Finally the resulting products were annealed at 800 °C for 10 h under N_2 flow of 0.7 L min^{-1}.

Powder X-ray diffraction (XRD) measurements were carried out on a Bruker D8 X-ray diffractometer with Cu Ka radiation monitored by graphite. The scan data were collected between 10 and 60 °C with a step interval of 0.02°. The morphological characteristics of the samples were analyzed by a JEOL JSM-6390 scanning electron microscopy (SEM) and a JOEL JEM2010 transmission electron microscope (TEM). The conductivity of the disc-shaped pellets of the synthesized materials was measured using a Solartron instruments model 1287 electrochemical interface controlled by a computer. The particle size distribution was measured by a dynamic light scattering particle size analyzer (Malvern Zetasizer Nano). The Brunauer, Emmett, and Teller (BET) method was used to measure the surface area of the powders (a Quantachrome ASiQwin).

The $LiFe_{0.2}Mn_{0.8}PO_4$ and $Li_4Ti_5O_{12}$ electrodes were both prepared by mixing 80 wt% active material, 10 wt% acetylene black as conductive material, and 10 wt% polyvinylidene difluoride (PVDF) binder in *N*-methyl-2-pyrrolidone (NMP) solvent. Then, the slurry was cast onto an aluminum foil current collector, punched in the form of disks typically with a diameter of 12 mm, and then dried at 80*C* for 12 h under vacuum before assembly. The typically mass loading of C-$LiFe_{0.2}Mn_{0.8}PO_4$ is about 9 mg cm^{-2}. The typical mass loading of C-$Li_4Ti_5O_{12}$ is about 6 mg cm^{-2}. The half-cell consists of C-$LiFe_{0.2}Mn_{0.8}PO_4$ cathode material, a separator, and metallic lithium anode. The full-cells contains of C-$LiFe_{0.2}Mn_{0.8}PO_4$ cathode, a separator, and C-$Li_4Ti_5O_{12}$ anode. Electrochemical measurements of both cells were carried out in CR2016-type coin cells

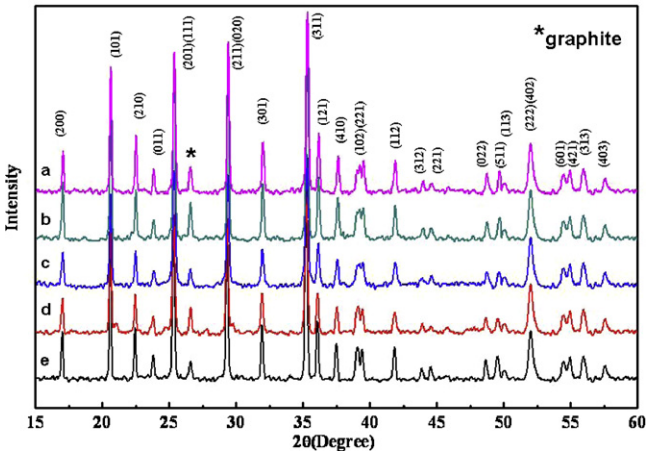

Fig. 1. XRD patterns of $LiFe_{0.2}Mn_{0.8}PO_4$ powder with different ratio between carbon black and sucrose: (a) 10:0, (b) 7:3, (c) 5:5, (d) 3:7, and (e) 0:10.

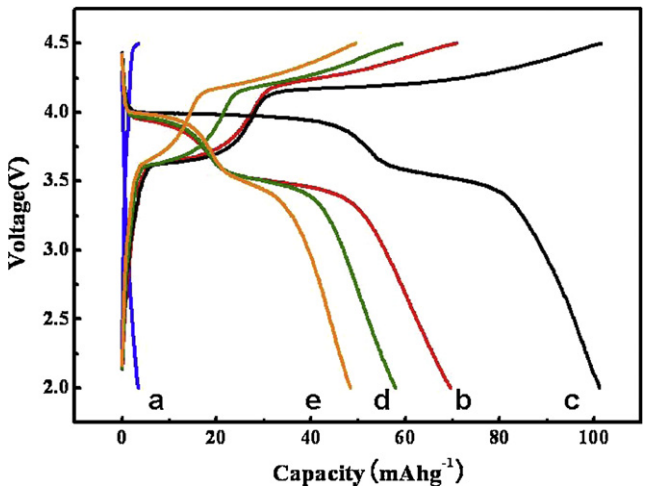

Fig. 2. Typical charge/discharge curves of Li/$LiFe_{0.2}Mn_{0.8}PO_4$ cells with different ratios of carbon black and sucrose between 2.0 and 4.5 V at a rate of 0.2*C*: (a) 10:0, (b) 7:3, (c) 5:5, (d) 3:7, and (e) 0:10.

at room temperature. The cells were assembled in a glove box filled with pure argon. The electrolyte solution was 1 M $LiPF_6$-ethylene carbonate (EC)/diethyl carbonate (DMC)/ethyl methyl carbonate (EMC) (1:1:1 by vol.). The specific capacity of the $LiFe_{0.2}Mn_{0.8}PO_4$ and $Li_4Ti_5O_{12}$ is calculated on the basis of the pure weight of the active material, and the capacity for the full cell referred to the total weight of both cathode and anode materials. The effects of carbon content on the electrolyte/$LiFe_{0.2}Mn_{0.8}PO_4$ interface resistances were also evaluated by monitoring the dependence of the impedance response on the carbon contents at the charge states (c.a. 60 mAh g^{-1} at 4.1 V). The experiments were carried out using a three-electrode cell, in which the lithium metal was used as both the counter and reference electrodes, and it was performed using a Solartron Instruments model 1287 electrochemical interface and 1255B frequency response analyzer controlled by a computer. The frequency limits were typically set between 1000 kHz and 0.01 Hz. The ac oscillation was 10 mV.

3. Results and discussion

3.1. Synthesis of C-$LiFe_{0.2}Mn_{0.8}PO_4$

3.1.1. Synthesis C-$LiFe_{0.2}Mn_{0.8}PO_4$ using different ratio of carbon source

As demonstrated in several previous studies, the sucrose was used to protect Fe^{2+} from oxidation and particle aggregation during the calcination process in preparing $LiFePO_4$. The sucrose was also chosen as a carbon precursor to synthesize $LiFe_{0.2}Mn_{0.8}PO_4$. On the other hand, adding carbon black (CB) improved the electronic conductivity of $LiFe_{0.2}Mn_{0.8}PO_4$ effectively.

The C-$LiFe_{0.2}Mn_{0.8}PO_4$ composites were prepared at different ratios of CB to sucrose. The total carbon content in the composites was controlled to 10 wt%. The carbonization rate of sucrose is 20%. The ratio in the following discussion refers to the ratio between the carbonized sucrose and the black carbon. Fig. 1 shows the X-ray diffraction (XRD) patterns of $LiFe_{0.2}Mn_{0.8}PO_4$ powders with different ratios of CB to sucrose: 10:0, 7:3, 5:5, 3:7 and 0:10. All diffraction peaks can be clearly indexed as olivine-type $LiFe_{0.2}Mn_{0.8}PO_4$ with a Pnmb space group of the orthorhombic system. No significant change in the lattice parameters was observed in these four samples.

Fig. 2 shows the charge/discharge curves of the C-$LiFe_{0.2}Mn_{0.8}PO_4$ with different ratios of CB to sucrose. The cell was charged/discharged between 4.5 and 2.5 V at a 0.2*C* rate.

The specific capacity of C-$LiFe_{0.2}Mn_{0.8}PO_4$ depends critically on the ratio between CB and sucrose. It is clear that C-$LiFe_{0.2}Mn_{0.8}PO_4$ delivers the largest specific capacity of 104 mAh g^{-1} at the ratio of 5:5 between CB and sucrose while the specific capacity decreases at both high and low content of CB; the specific capacities for the samples with the ratio of CB to sucrose at 7:3 and 3:7 are 70 mAh g^{-1} and 59 mAh g^{-1}, respectively. The sample obtained from pure CB precursor solely delivers a capacity of 5 mAh g^{-1}. The very low capacity is mainly because of the oxidation of Mn^{2+} during the preparation of the sample without sucrose. The sample obtained from pure sucrose carbon precursor also delivers a smaller capacity of 48 mAh g^{-1}, which is mainly due to low electronic conductivity of the carbon layer calcinated at low temperature.

3.1.2. Influence of the ball milling on synthesis

It is well known that the specific capacity and rate capability scale with the particle size, especially for the olivine structure compounds with a low lithium diffusion coefficient. The specific capacity of $LiFe_{0.2}Mn_{0.8}PO_4$ can be improved by preparing particles with a smaller size. We employed a high-energy ball-milling process to study the effect of the ball-milling time on its particle size and charge/discharge profile. C-$LiFe_{0.2}Mn_{0.8}PO_4$ containing 5% carbonized sucrose and 5% BC was chosen as a starting material. Fig. 3 shows the X-ray diffraction (XRD) patterns of $LiFe_{0.2}Mn_{0.8}PO_4$ powders with different ball milling times: 2.5 h, 5 h, 10 h and 18 h. All diffraction peaks could be clearly indexed as olivine-type $LiFe_{0.2}Mn_{0.8}PO_4$ with a Pnmb space group of the orthorhombic system. No significant change in the lattice parameters was observed with an increasing time of ball milling. Fig. 4 presents scanning electron microscopy (SEM) images of the $LiFe_{0.2}Mn_{0.8}PO_4$ with different ball milling times. As can be seen from the SEM images, the particle size obviously decreased during the first several hours of ball milling before finally saturating. This result was further confirmed by particle size distribution (PSD) measurement. The particle size of sample A decreased from 500 nm to 165 nm during 2.5 h of ball milling and further decreased to 105 nm after 5 h

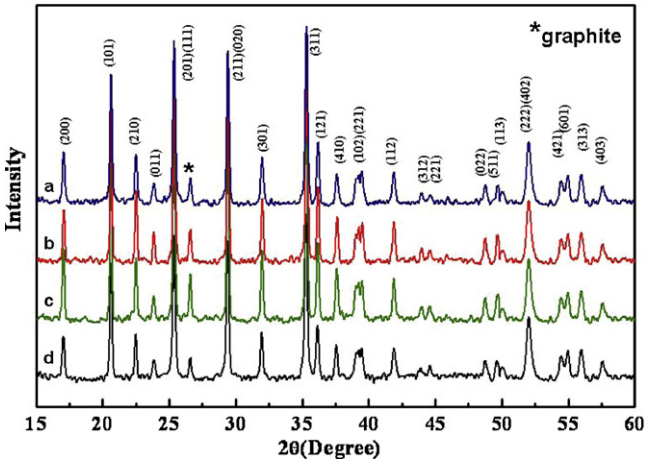

Fig. 3. XRD patterns of $LiFe_{0.2}Mn_{0.8}PO_4$ powders with different times of ball milling: (a) 2.5 h, (b) 5 h, (c) 10 h, and (d) 18 h.

of ball milling. The particle increases again to a size of 120 nm and 154 nm at a ball milling time of 10 h and 18 h, respectively.

The charge–discharge curves of the $LiFe_{0.2}Mn_{0.8}PO_4$ at different ball milling times are presented in Fig. 5. The capacity of the $LiFe_{0.2}Mn_{0.8}PO_4$ electrode was determined between 4.5 and 2.5 V by galvanostatic charge/discharge testing at a rate of 0.2*C*. As expected, sample B, which has the smallest particle size, has the largest capacity of 110 mAh g^{-1}. The discharge capacity decreased to 68 mAh g^{-1}, 99 mAh g^{-1} and 80 mAh g^{-1} at the ball milling time of 2.5, 10 and 18 h, respectively. The capacity scales with the particle size.

3.1.3. Effect of the total carbon content on synthesis

The effect of the total carbon content on the electrochemical properties of C-$LiFe_{0.2}Mn_{0.8}PO_4$ was extensively studied. The samples were prepared using a ratio for CB and sucrose of 5:5 with 5 h of ball milling. The total carbon content was controlled from 10 wt%

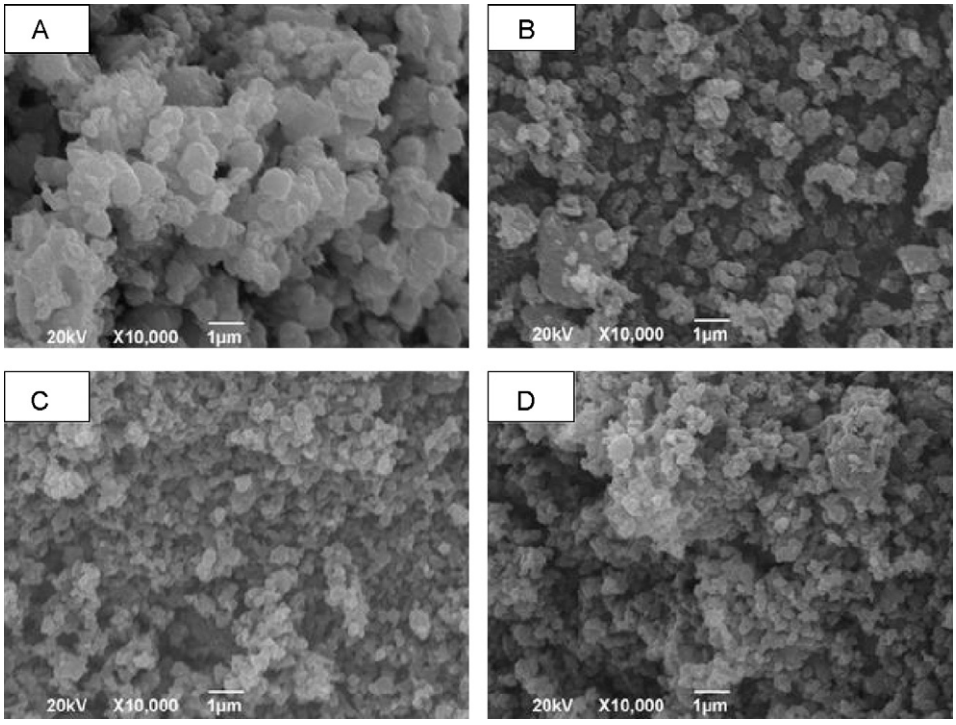

Fig. 4. SEM images of $LiFe_{0.2}Mn_{0.8}PO_4$ powders with different times of ball milling: (a) 2.5 h, (b) 5 h, (c) 10 h, and (d) 18 h.

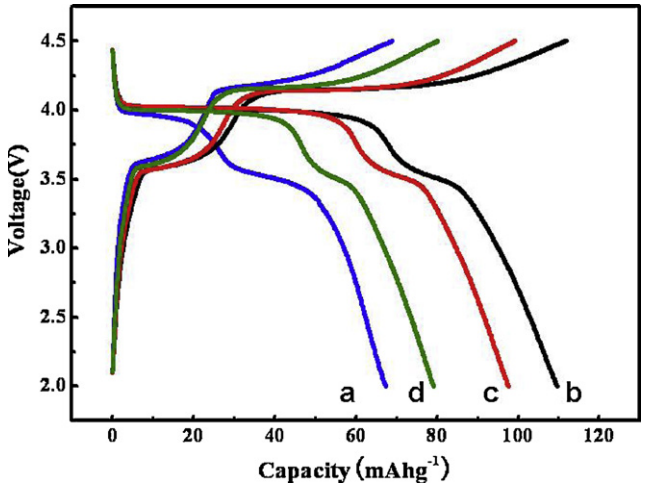

Fig. 5. Typical charge/discharge curves of Li/$LiFe_{0.2}Mn_{0.8}PO_4$ cells with different ball-milling times between 2.0 and 4.5 V at a rate of 0.2C: (a) 2.5 h, (b) 5 h, (c) 10 h, and (d) 18 h.

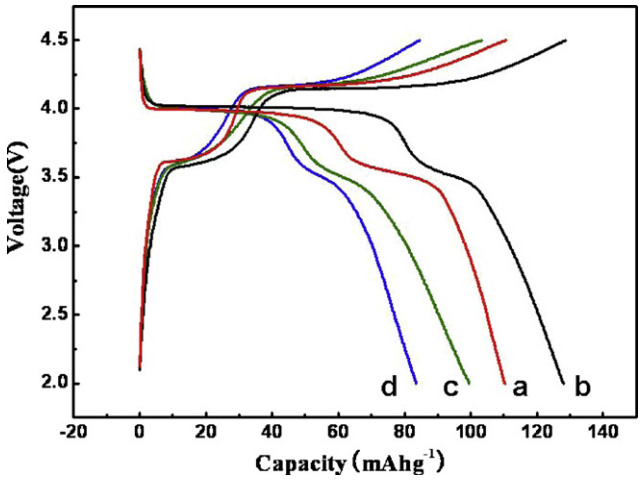

Fig. 7. Charge/discharge curves of Li/$LiFe_{0.2}Mn_{0.8}PO_4$ cells with different amount of carbon between 2.0 and 4.5 V at a rate of 0.2C: (a) 10%, (b) 20%, (c) 30%, and (d) 40%.

to 20, 30, and 40 wt%. Fig. 6 shows scanning electron microscopy (SEM) images of the $LiFe_{0.2}Mn_{0.8}PO_4$ powder with different carbon contents. The images show that the $LiFe_{0.2}Mn_{0.8}PO_4$ powder is composed of agglomerated nanoparticles. As shown in Fig. 6a, the average grain size of $LiFe_{0.2}Mn_{0.8}PO_4$ nanoparticles is about 100 nm. Ball-shaped accumulation occurs when the carbon content increases to 20%. With a further increase of carbon content, there is a greater accumulation of small balls.

Fig. 7 shows typical charge–discharge curves of the $LiFe_{0.2}Mn_{0.8}PO_4$ cells with various amounts of carbon (10–40 wt%). Specific capacity was found to be highly dependent on the particle size. The discharge capacities increased from 110 mAh g^{-1} to 129 mAh g^{-1} when the carbon content was increased from 10 to 20 wt%. The discharge capacity decreased to 102 mAh g^{-1} at a carbon content of 30 wt% and to 84 mAh g^{-1} at a carbon content of 40 wt%. It is important to note that the sample with 20% total carbon exhibits an excellent capability. Given these results, we measured the electronic conductivity of these materials. The results are summarized in Table 1. Generally, the samples with higher carbon content show a higher electronic conductivity, which consequently tends to exhibit a higher capacity. However, an excessive amount of carbon, as seen in the cases for more than 30 wt% in Table 1, caused carbon particle segregation, which impeded the electron transport and decreased the electrical

Table 1
Conductivity of $LiFe_{0.2}Mn_{0.8}PO_4$ powders with different amounts of carbon.

	a	b	c	d
Carbon content	10%	20%	30%	40%
Conductivity (S cm^{-1})	3.6	5.1	3.1	2.9
Capacity (mAh g^{-1})	110	129	102	84

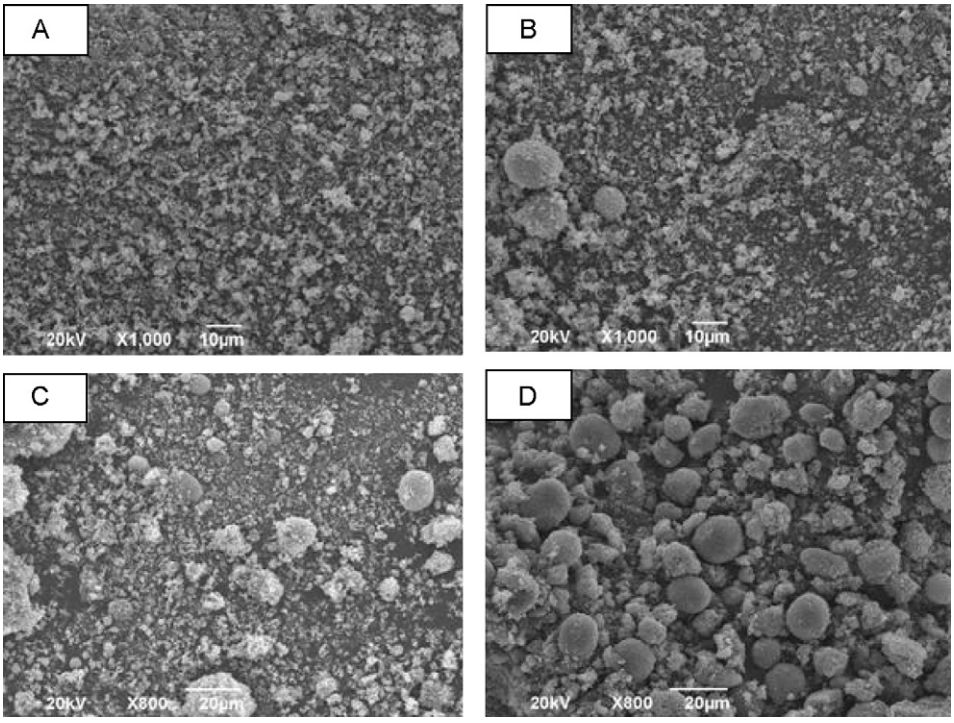

Fig. 6. SEM images of $LiFe_{0.2}Mn_{0.8}PO_4$ powders with different amounts of carbon: (a) 10%, (b) 20%, (c) 30%, and (d) 40%.

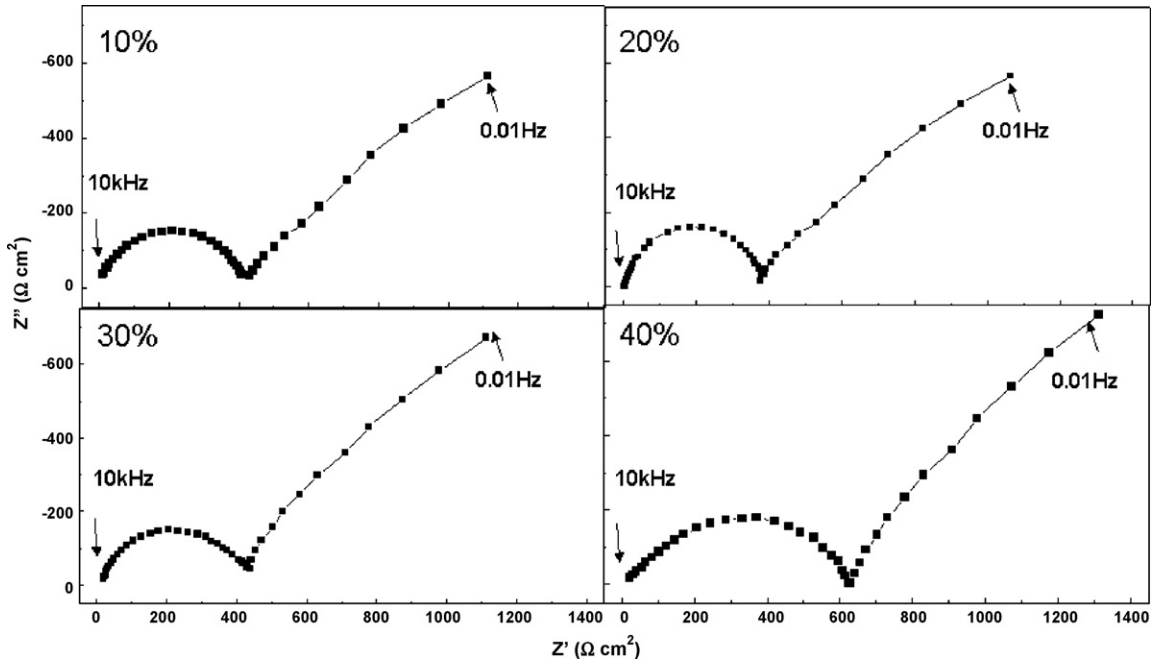

Fig. 8. AC impedance plots of $LiFe_{0.2}Mn_{0.8}PO_4$ electrodes with different amount of carbon.

conductivity of the material. Hence, the SEM results and electrical measurements indicate that the optimum microstructure occurs at 20 wt% carbon content and that a further addition of carbon leads to the deterioration of the electrical conductivity due to carbon segregation.

It should be noted that Li^+ intercalation involves an acceptance of Li^+ ion in the particle surface/electrolyte interface accompanied by accepting an electron. The reaction can only occur on the selected spots in which both the electrical conductive and Li^+ ion diffusion path are built. The rate capability depends on both the electronic and ionic conductivity. We carried AC impedance to determine the difference in the charge-transfer resistance for four samples with different carbon contents. The results for AC impedance are displayed in Fig. 8 typically one dispersed semicircle and line approximating to 45 °C within the frequency range 10^5 Hz to 0.01 Hz was observed. The dispersed semicircle includes two overlapped semicircles. The total impedance could be considered the surface film impedance in the high frequency which can be represented by a surface film resistance, R_{sf} in parallel with a capacitance, $C_{sf,}$ and the impedance in the medium frequency contributed from the charge-transfer process, which can be characterized by $R_{ct_{Li+}}$ and CPE combination, where $R_{ct_{Li+}}$ is charge-transfer resistance, and CPE can be considered as the double-layer capacitance, C_{dl} [23,24]. The equivalent circuits are also given in the Fig. 9. The fitting results including internal resistance, R_i, surface film resistance, $R_{sf,}$ lithium-ion intercalation charge-transfer resistance and $R_{ct_{Li+}}$ are summarized in Table 2. As the results show in the Table 2, the sample of 20% carbon shows the smaller interfacial charge-transfer resistance.

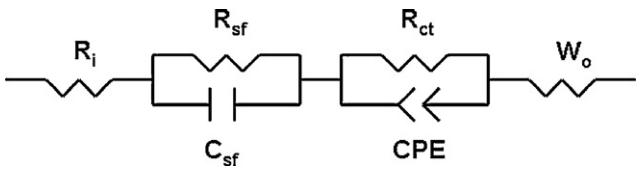

Fig. 9. Equivalent circuit model of the studied system.

Table 2
Summaries of the fitting results of internal resistances (R_i), surface film resistance (R_{sf}), and charge-transfer resistances for Li^+ intercalation (R_{ct}) based on a series of experimental results.

Electrodes	R_i (Ω)	R_{sf} (Ω)	R_{ct} (Ω)
10%	5.36	5.15	10.8
20%	4.21	4.983	5.257
30%	3.122	4.515	8.798
40%	5.43	8.492	10.55

From the above examinations, the optimal synthesis of $LiFe_{0.2}Mn_{0.8}PO_4$ was performed at 550 °C for 3 h with a ratio for the carbon precursor of CB and sucrose of 5:5 (total carbon content of 20 wt%) with ball-milling for 5 h.

3.2. Electrochemical properties

3.2.1. Performance of $Li/LiFe_{0.2}Mn_{0.8}PO_4$ half cells

The XRD pattern of $LiMn_{0.8}Fe_{0.2}PO_4$ prepared under optimal conditions is shown in Fig. 10. The diffraction peaks belong to an

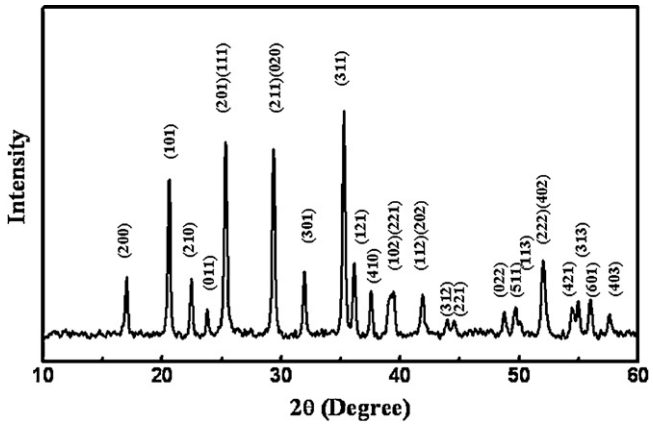

Fig. 10. Typical XRD pattern of $LiFe_{0.2}Mn_{0.8}PO_4$ nanoparticles.

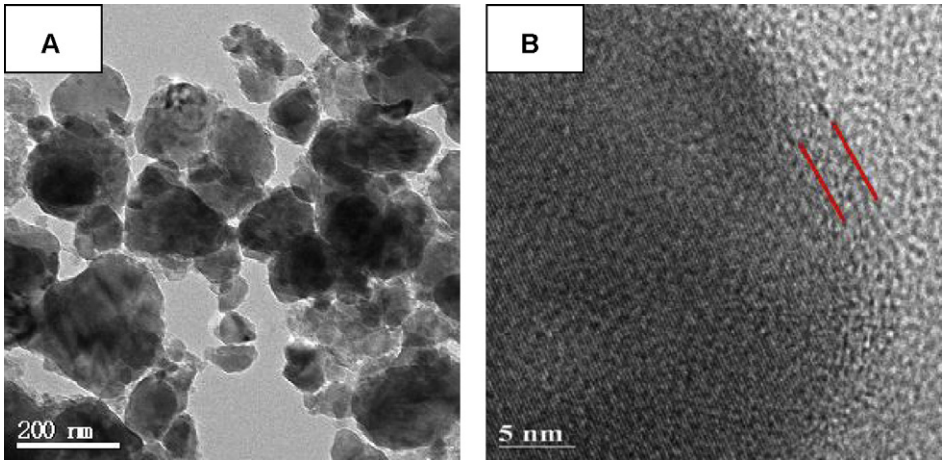

Fig. 11. TEM micrographs of nanoparticles of $LiFe_{0.2}Mn_{0.8}PO_4$.

ordered olivine indexed by orthorhombic structure space group Pnma with lattice parameters of $a = 10.4244$, $b = 6.0902$, $c = 4.7315$, and cell volume, $V = 300.8304$, which is consistent with the previous results reported by Yamada et al. [16]. The TEM image in Fig. 11a shows that the particle size is less than 100 nm. Moreover, a 4 nm thick carbon layer was uniformly coated on the surface of the particle (Fig. 11b). The specific surface is 90.7 $m^2\,g^{-1}$ measured by N_2 absorption on the BET model.

Typical charge–discharge profiles of prepared $LiFe_{0.2}Mn_{0.8}PO_4$ at different temperatures were measured at 0 °C, 25 °C, and 60 °C. The results are shown in Fig. 12. $LiFe_{0.2}Mn_{0.8}PO_4$ show two expected plateaus at about 4.1 V and 3.5 V (versus the Li reference electrode) at both room temperature and elevated temperatures in the discharge process, which are related to the Mn^{2+}/Mn^{3+} and the Fe^{2+}/Fe^{3+} redox couples. Specific discharge capacities are 151 mAh g^{-1} and 130 mAh g^{-1} at 60 °C and 25 °C, respectively. When the temperature was decreased to 0 °C, the capacity significantly decreased to 60 mAh g^{-1}. The poor capacity at low temperature is most likely due to the low lithium diffusion in the bulk material and slow lithium-ion transport in the electrolyte.

The rate capability performance, especially at a high rate, is another important aspect for the application of manganese-based olivine cathodes for EV/HEV power sources aside from the cycling performance. Fig. 13a shows the discharge capacity of carbon-coated $LiFe_{0.2}Mn_{0.8}PO_4$ at different current rates, varying from 0.05*C* to 10*C*. At 10*C* rate, carbon-coated $LiFe_{0.2}Mn_{0.8}PO_4$ maintains about 45% of its capacity compared with the capacity at a rate of 0.05*C*. This result demonstrates that the suitable carbon coat and particle size may facilitate the fast transport and intercalation kinetics of lithium ions, even at a high charge–discharge current.

Fig. 13b shows the cycle performance of $LiFe_{0.2}Mn_{0.8}PO_4$ between potential limits of 2.0 and 4.5 V at a rate of 0.2*C*. Carbon-coated $LiFe_{0.2}Mn_{0.8}PO_4$ exhibits excellent cycling performance. It

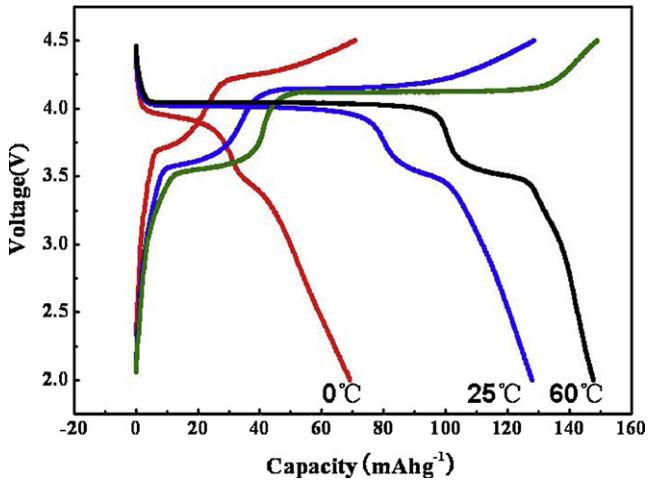

Fig. 12. Typical charge/discharge curves of Li/$LiFe_{0.2}Mn_{0.8}PO_4$ cells at different temperatures: (a) 60 °C, (b) 25 °C, and (c) 0 °C.

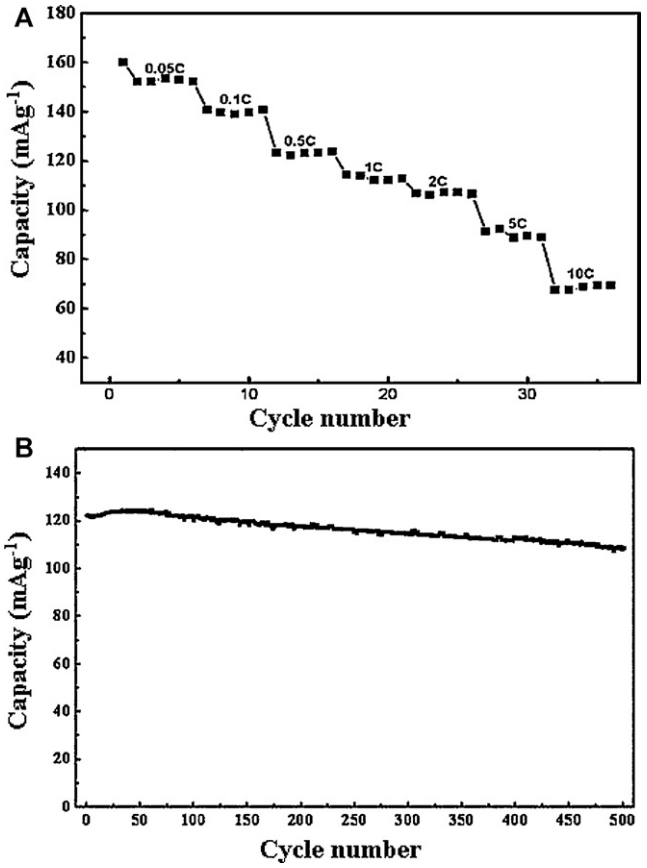

Fig. 13. (a) Capability at different rates of 0.05, 0.1, 0.5, 1, 2, 5, and 10*C*, and (b) cycling performance of Li/$LiFe_{0.2}Mn_{0.8}PO_4$ cells between 2.0 and 4.5 V at a current rate of 0.2*C*.

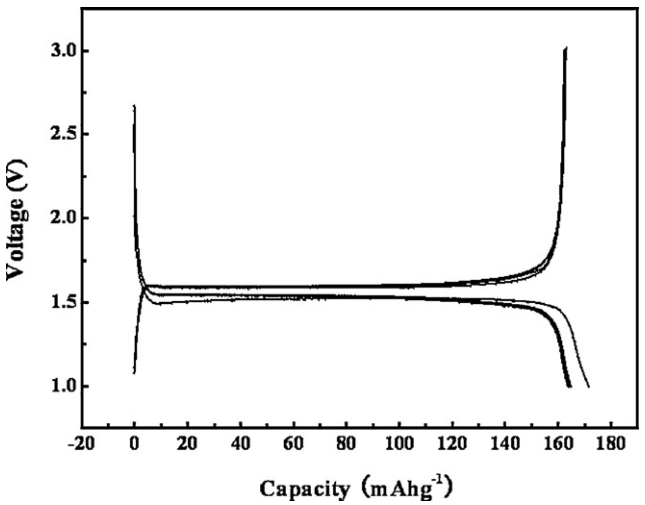

Fig. 14. Typical charge/discharge curves of $Li/Li_4Ti_5O_{12}$ cells between 1.0 and 3.0 V at a current rate of 0.2*C*.

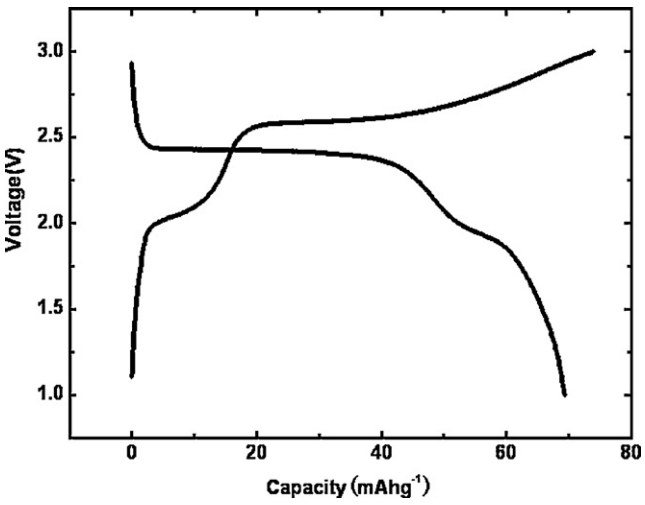

Fig. 15. Typical charge/discharge curves of $LiFe_{0.2}Mn_{0.8}PO_4/Li_4Ti_5O_{12}$ full-cell between 1.0 and 3.0 V at a rate of 0.1*C*.

shows a slow capacity that fades upon cycling with an average capacity loss of no more than 0.02% per cycle. Carbon coated $LiFe_{0.2}Mn_{0.8}PO_4$ maintains 91% of its initial capacity after 500 cycles. To the best of our knowledge, it is the best cycling life of any reported $LiMnPO_4$.

3.2.2. Performance of $Li/Li_4Ti_5O_{12}$ half cells

$Li_4Ti_5O_{12}$ has been demonstrated to be the most promising anode material for lithium-ion batteries because it exhibits excellent Li-ion insertion/extraction reversibility with zero structural change and a relatively higher operating voltage (1.55 V vs. Li/Li^+) to ensure a safer battery and thus avoid the trouble of lithium dendrites. Considering the safety of the large scale battery for electric vehicles (EV) and the electric power utility applications, the cathode materials currently used for such batteries are the spinel structure $LiMn_2O_4$, and the olivine-type structure $LiFePO_4$. However, these batteries still have poor cycling stability at elevated temperatures due to Mn dissolution of $LiMn_2O_4$ and low specific energy due to low working voltage when combined with $LiFePO_4$ [25–27]. Using $LiMnPO_4$ cathode materials with a high voltage and good cycling would address these drawbacks. Fig. 14 displays a typical charge/discharge curve of the $Li_4Ti_5O_{12}$ nanoporous microsphere. The microsphere shows the reversible discharge capacity of 160 mAh g^{-1} with an initial coulombic efficiency of 95% at a rate of 0.2*C* (32 mAh g^{-1}). The detailed information concerning this material information can be found in our previous report [28].

3.2.3. Performance of Li $Fe_{0.2}Mn_{0.8}PO_4/Li_4Ti_5O_{12}$ full cells

Fig. 15 shows the charge and discharge curves of the $LiFe_{0.2}Mn_{0.8}PO_4/Li_4Ti_5O_{12}$ full cell between 1.0 and 3.0 V at a current rate of 0.1*C*. The balancing mass ratio of anode and cathode materials was designed to be 1:1.5 by using the specific capacity of 160 mAh g^{-1} of C-$Li_4Ti_5O_{12}$ and 140 mAh g^{-1} of C-$LiFe_{0.2}Mn_{0.8}PO_4$, separately. The data in Fig. 14 clearly demonstrate that the $LiFe_{0.2}Mn_{0.8}PO_4/Li_4Ti_5O_{12}$ lithium-ion battery has a good capacity of 70 mAh g^{-1} and a specific energy of 170 Wh kg^{-1} with an output voltage of 2.45 V dependent on the total weight of both active electrode materials.

Fig. 16a displays the typical flat voltage profiles of a full cell at various discharge rates between 0.1*C* and 5*C*. Typically, the $LiFe_{0.2}Mn_{0.8}PO_4/Li_4Ti_5O_{12}$ full cells studied herein exhibit an initial discharge capacity of 70 mAh g^{-1} at low rates of 0.1*C*; more than 58 mAh g^{-1} and 40 mAh g^{-1} of discharge capacity was delivered at a rate of 0.5*C* and 2*C*, respectively. The cell showed good rate capability, maintaining a capacity of 30 mAh g^{-1}, when cycled at various rates up to 5*C*, in corresponding to a capacity retention of 50% compared with that of 0.1*C* rate. Fig. 16b gives the cycling life test of $LiFe_{0.2}Mn_{0.8}PO_4/Li_4Ti_5O_{12}$ full cells between 1.0 V and 3.0 V at discharge rate of 0.1*C*. The cell indicates very good cycling stability with a capacity retention of 92% over 200 charge/discharge cycles.

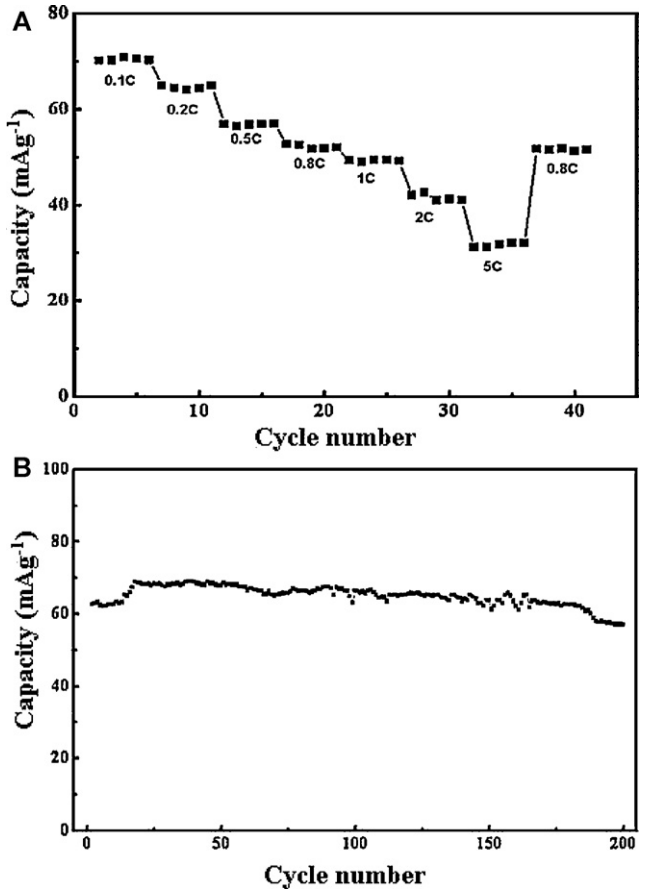

Fig. 16. (a) Capability at different rates: 0.1, 0.2, 0.5, 0.8, 1, 2, and 5*C*, and (b) cycling performance of $LiFe_{0.2}Mn_{0.8}PO_4/Li_4Ti_5O_{12}$ full cells between 1.0 and 3.0 V at a rate of 0.1*C*.

4. Conclusion

$LiFe_{0.2}Mn_{0.8}PO_4$ was prepared by a solid state reaction process in combination with a ball-milling with carbon black and sucrose as carbon sources. The optimal condition for preparation of $LiFe_{0.2}Mn_{0.8}PO_4$ was performed at 550 °C for 3 h using both CB and sucrose precursor (5:5 in ratio, total carbon content of 20 wt%) with ball-milling for 5 h. The as-prepared $LiFe_{0.2}Mn_{0.8}PO_4$ gives a capacity of 150 mAh g^{-1} at 1/20*C* and 110 mAh g^{-1} at 1*C*. This is because that the suitable carbon coat and particle size may facilitate the fast transport and intercalation kinetics of lithium ions, even at a high charge–discharge current. A novel lithium-ion battery consisting of $LiFe_{0.2}Mn_{0.8}PO_4$ cathode, $Li_4Ti_5O_{12}$ anode delivers a specific energy of 170 Wh kg^{-1} with an output voltage of 2.45 V based on the total weight of both active electrode materials. The cell also exhibits an excellent cycling stability with a capacity retention of 92% over 200 charge/discharge cycles. The battery described in the present work may give the most promising potential for the EV and stationary power source applications due to the relative high energy density, low cost and long cycling life.

Acknowledgments

This work was partially supported by the National Natural Science Foundation of China (20925312), the State Key Basic Research Program of PRC (2011CB935903), and Shanghai Science & Technology Committee (10JC1401500, 08DZ2270500).

References

[1] A. Padhi, K.S. Nanjundaswamy, J.B. Goodenough, J. Electrochem. Soc. 144 (1997) 1188.
[2] A. Padhi, K.S. Nanjunclaswamy, C. Masquelier, S. Okada, J.B. Goodenough, J. Electrochem. Soc. 144 (1997) 1609.
[3] S.Y. Chung, J.T. Blocking, Y.M. Chiang, Nat. Mater. 1 (2002) 123.
[4] P.P. Prosini, M. Lisi, D. Zane, M. Pasquali, Solid State Ionics 45 (2002) 148.
[5] C. Delacourt, L. Laffont, R. Bouchet, C. Wurm, J.B. Leriche, M. Morcette, J.M. Tarascon, C. Masquelier, J. Electrochem. Soc. 152 (2005) A913.
[6] G. Rousse, J. Rodriguez-Carvajal, S. Patoux, C. Masquelier, Chem. Mater. 15 (2003) 4082.
[7] G. Li, H. Azuma, M. Tohda, Electrochem. Solid-State Lett. 5 (2002) A135.
[8] N.-H. Kwon, T. Drezen, I. Exnar, I. Teerlinck, M. Isono, M. Grätzel, Electrochem. Solid-State Lett. 9 (2006) A277.
[9] T. Drezen, N.-H. Kwon, P. Bowen, I. Teerlinck, M. Isono, I. Exnar, J. Power Sources 174 (2007) 949.
[10] S.K. Martha, B. Markovsky, J. Grinblat, Y. Gofer, O. Haik, E. Zinigrad, D. Aurbach, T. Drezen, D. Wang, G. Deghenghi, I. Exnar, J. Electrochem. Soc. 156 (2009) A541.
[11] J. Xiao, W. Xu, D. Choi, J.-G. Zhang, J. Electrochem. Soc. 157 (2010) A142.
[12] C. Delacourt, P. Poizot, M. Morcrette, J.M. Tarascon, C. Masquelier, Chem. Mater. 16 (2004) 93.
[13] D. Wang, H. Buqa, M. Crouzet, G. Deghenghi, T. Drezen, I. Exnar, N.-H. Kwon, J.H. Miners, L. Poletto, M. Grätzel, J. Power Sources 189 (2009) 624.
[14] Z. Bakenov, I. Taniguchi, Electrochem. Commun. 12 (2010) 75.
[15] A. Yamada, Y. Kudo, K.Y. Liu, J. Electrochem. Soc. 148 (2001) A747.
[16] A. Yamada, S.C. Chung, J. Electrochem. Soc. 148 (2001) A960.
[17] S.K. Martha, J. Grinblat, O. Haik, E. Zinigrad, T. Drezen, J.H. Miners, I. Exnar, A. Kay, B. Markovsky, D. Aurbach, Angew. Chem. Int. Ed. 48 (2009) 8559.
[18] B. Zhang, X.J. Wang, Z.J. Liu, H. Li, X.J. Huang, J. Electrochem. Soc. 157 (2010) A285.
[19] M. Gaberscek, R. Dominko, M. Bele, M. Remskar, D. Hanzel, J. Jamnik, Solid State Ionics 176 (2005) 1801.
[20] T. Ohzuku, Y. Iwakoshi, K. Sawai, J. Electrochem. Soc. 140 (1993) 2490.
[21] J.K. Kim, G. Cheruvally, J.H. Ahn, J. Solid State Electrochem. 12 (2008) 799.
[22] S.M. Oh, S.W. Oh, C.S. Yoon, B. Scrosati, K. Amine, Y. Sun, Adv. Funct. Mater. 20 (2010) 3260.
[23] J. Wolfenstine, U. Lee, J.L. Allen, J. Power Sources 154 (2006) 287.
[24] L. Cheng, X.L. Li, H.J. Liu, H.M. Xiong, P.W. Zhang, Y.Y. Xia, J. Electrochem. Soc. 154 (2007) A692.
[25] T. Ohzuku, A. Ueda, N. Yamamoto, J. Electrochem. Soc. 142 (1995) 1431.
[26] K. Zaghib, M. Simoneau, M. Armand, M. Gauthier, J. Power Sources 300 (1999) 81.
[27] Y.H. Rho, K. Kanamura, M. Fujisaki, J.-I. Hamagami, S.-I. Suda, T. Umegaki, Solid State Ionics 151 (2002) 151.
[28] G.N. Zhu, H.J. Liu, J.H. Zhuang, C.X. Wang, Y.G. Wang, Y.Y. Xia, Energy Environ. Sci. 10 (2011) 4016.